View metadata, citation and similar papers at core.ac.uk

brought to you by CORE

provided by Elsevier - Publisher Connector

Available online at www.sciencedirect.com

ScienceDirect

Procedia CIRP 37 (2015) 89 – 94

www.elsevier.com/locate/procedia

CIRPe 2015 - Understanding the life cycle implications of manufacturing

Modeling of formation of nanostructured metal surfaces by electrodeposition through a monolayer colloidal crystal mask

V.M. Volgin[a,]*, V.V. Lyubimov[a], I.V. Gnidina[a], A.D. Davydov[b]

[a]*Tula State University, pr. Lenina 92, Tula 300012, Russia*
[b]*Frumkin Institute of Physical Chemistry and Electrochemistry RAS, Leninskii pr. 31, Moscow 119071, Russia*

* Corresponding author. Tel.: +7-4872-35-24-52; fax: +7-4872-35-81-81. *E-mail address:* volgin@tsu.tula.ru

Abstract

Electrochemical deposition is a feasible and well-controlled method for the formation of various micro- and nanostructures. A rich variety of periodical nanostructures of functional materials with multi-shaped and tunable morphologies can be fabricated by the electrochemical deposition, in particular, using monolayer colloidal crystal (MCC) mask. A mathematical model of the mass-transfer processes and deposit surface evolution during the metal electrodeposition through MCC mask is presented. The mathematical model involves the equations for the potential and deposit surface evolution. The problem was solved numerically by the boundary element method, and the "Level Set" method. The numerical experiments were used to study the effect of parameters, which characterize the mask geometry and the process conditions, on the initial distribution of current density over the deposit surface and the variation of current density distribution in the course of the deposition.

© 2015 The Authors. Published by Elsevier B.V. This is an open access article under the CC BY-NC-ND license (http://creativecommons.org/licenses/by-nc-nd/4.0/).

Peer-review under responsibility of the organizing committee of CIRPe 2015 - Understanding the life cycle implications of manufacturing

Keywords: Electrodeposition; Colloidal Crystal Mask; Numerical simulation

1. Introduction

The understanding of surface phenomena at a micro- and nanometer scale, has played a fundamental role in the many fields, such as: electronics, energy, optics, tribology, biology, biomimetics, etc. [1]. The manufacturing of features on the nanometer scale is challenging, and has been the subject of intensive research and development [2] The relationships between the technologies for structuring surfaces, their functional properties (improved adhesion, superhydrophobicity, antireflection and other optical properties, generation and preservation of energy, hard and tough surfaces, efficient heat transfer, antibiofouling, changing color, and self-healing) and the applications exploiting the surface functionality are a common denominator of the research carried out in the last years [3].

The template-based methods occupy a prominent place among various methods of production of nanostructures and nanostructured materials [4]. These methods enable one to fabricate the desired material in the pores of nanoporous template.

Nomenclature

d_{SP}	diameter of spherical particles
h	height of unit cell
H	dimensionless height of unit cell
i_0	applied current density
k	number of computational point
n	number of time step
$\mathbf{N}$	unit vector of outer normal to surface
R	dimensionless radius of spherical particles
t	time
x, y, z	coordinates
X, Y, Z	dimensionless coordinates
z_c	function, which describes deposit surface
Z_c	dimensionless function, which describes deposit surface
ε_V	volumetric electrochemical equivalent
η	current efficiency
τ	dimensionless time
$\Delta\tau$	dimensionless time step
φ	potential

2212-8271 © 2015 The Authors. Published by Elsevier B.V. This is an open access article under the CC BY-NC-ND license (http://creativecommons.org/licenses/by-nc-nd/4.0/).

Peer-review under responsibility of the organizing committee of CIRPe 2015 - Understanding the life cycle implications of manufacturing
doi:10.1016/j.procir.2015.08.095

χ	conductivity of electrolyte solution
Φ	dimensionless potential
C	subscript, which denotes deposit surface
U	subscript, which denotes outer boundary of unit cell
I	subscript, which denotes side surfaces of unit cell and surface of spherical particle

Various methods can be used for the template-based synthesis of nanoporous structures: the chemical polymerization, sol-gel deposition, chemical vapor deposition and also the electrochemical and electroless deposition and electrochemical dissolution [5].

The template-based electrochemical methods of synthesis of nanostructures and nanomaterials have several important advantages: a high extent of pore filling, a possibility to obtain the materials of various types, the absence of considerable internal stresses, easy control, a possibility to vary the physicochemical properties and composition of the deposit. For example, the electrochemical methods enable one to produce heterogeneous nanostructured materials for the electrochemical power sources, fuel cells, and catalyst for various purposes [6].

Solid templates of polycarbonate track membranes or nanoporous aluminum oxide with linear pores 50-200 nm in diameter and 10-50 μm in depth are used most commonly [7]. They are used to produce the 1D structures of various materials: the metal nanowire arrays [8], the nanowires of various metal compounds [9]. Using the developed technologies, the electrochemical deposition of metals, alloys, and various chemical compounds in the pores of these templates is performed in order to fabricate modern miniature devices of magnetic memory, optoelectronics, sensors, power sources, supercapacitors, catalysts, and various electronic devices. The deposition of iron, nickel, or cobalt for fabrication of unique one-dimensional magnetic structures and also copper, ZnO, Ag_7Te_4, Co-Sb, MnO_2, Cu_3Se_2, Bi, Pt-Pb, Fe-Pt, Ni-Pt, Co-Pt, Si, $LaMnO_{3+\delta}$, etc. are examples. Solis templates are also used to produce bimetal and composite nanowires, which exhibit unique properties. For example, the electrodeposition at an electrode potential varying with time is used to fabricate the nanowires consisting of alternating copper and cobalt layers, where the effect of giant magnetic resonance is observed [7]. This method is also used to produce the structures of core-shell type and segmented metal-polymer composites [10].

Among other template structures, the templates consisting of regularly arranged monodispersed spherical particles are of most interest. They are used to produce composite materials, photon crystals, the structures with highly developed surface, for example, metal foams, for modification of surface properties, etc.

Colloidal crystals, which are formed by orderly arranged monodispersed spherical particles, are used as the templates for production of nano-ordered structures of metals, semiconductors, inorganic oxides, polymers, etc. [11]. In general case, the production of nano-ordered structures by using the colloidal crystal mask involves three stages:

(1) self-assembling of mask on the substrate surface;

(2) filling the pores between the template spherical particles;

(3) removal of template by chemical or thermal etching. (In some cases, for example, in the production of photonic crystals, the template is not removed.)

The 3D (multilayer) [12] and 2D (monolayer) [13] colloidal crystals are used as the masks. The MCC masks can be close-packed [14] or consist of regularly arranged non-close-packed particles [15].

The electrochemical deposition through a colloidal crystal mask enables one to produce high-density metal deposits, which exhibit no considerable shrinkage when the template is removed [16]. In addition, the deposits of various metals with prescribed structure can be produced, and the thickness and properties of deposited layer can be controlled accurately [17]. The application of a layer of metal or alloy, which acts as a catalyst for a chemical reaction, is the most important application of the process. An example is the application of a layer of relatively expensive platinum catalyst with developed (rough) surface onto a plane substrate of inexpensive material, such as iron.

To our knowledge, the electrodeposition through a colloidal crystal mask was investigated theoretically by the numerical simulation using the finite element method only in few works [18, 19].

In these papers the Laplace's equation in a unit cell with triangular cross-section for the face-centered cubic colloidal crystal was solved numerically. The process of pore filling and the variation of the mass-transfer conditions with increasing deposit thickness were not considered.

Here, we perform the numerical simulation of mass-transfer processes during the metal electrodeposition through a MCC mask with regard for the variation of deposited layer thickness with the time.

2. Statement of problem and basic equations

Figure 1 gives a scheme of metal electrodeposition with the use of monolayer colloidal crystal mask. Taking into account the arrangement of particles in the mask, a unit cell with a regular hexagonal cross-section is used (Fig. 2a). A plane, which is far removed from the mask, so that the distribution of the current density over this plane can be considered as uniform, is taken to be the outer (upper) boundary of a unit cell. The surface of growing metal deposit is taken to be the lower boundary of unit cell. The unit cell can be replaced by the axisymmetric one with no considerable error (Fig. 2b).

The Laplace equation for the electric field potential in the electrolyte solution (1) and the equation of deposit surface evolution (2) are used as the mathematical model:

$$\frac{\partial^2\varphi}{\partial x^2}+\frac{\partial^2\varphi}{\partial y^2}+\frac{\partial^2\varphi}{\partial z^2}=0 \tag{1}$$

$$\frac{\partial z_c}{\partial t}=-\eta\varepsilon_V\chi\frac{\partial\varphi}{\partial N}\sqrt{1+\left(\frac{\partial z_c}{\partial x}\right)^2+\left(\frac{\partial z_c}{\partial y}\right)^2} \tag{2}$$

For convenient numerical solution and analysis of obtained results, the mathematical model is presented in the dimensionless form. When passing to the dimensionless variables, the diameter of spherical particles d_{SP} is taken as a unit length and the applied current density i_0 is taken as a unit current density:

$$X=\frac{x}{d_{SP}},\ Y=\frac{y}{d_{SP}},\ Z=\frac{z}{d_{SP}},\ Z_c=\frac{z_c}{d_{SP}},\ H=\frac{h}{d_{SP}},\ \Phi=\frac{\chi\varphi}{i_0 h} \quad (3)$$

The dimensionless time is defined as follows:

$$\tau=\frac{\eta\varepsilon_V i_0 h}{d_{SP}^2}t \quad (4)$$

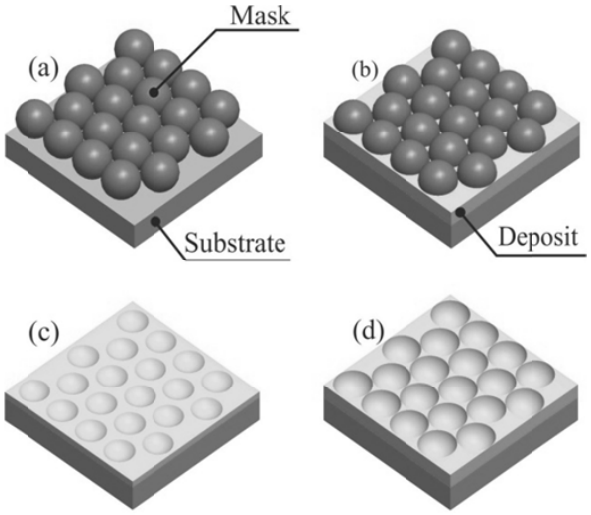

Fig. 1. Scheme of metal electrodeposition through monolayer colloidal crystal mask: (a) metal substrate with mask before electrodeposition; (b) metal substrate with mask in the course of electrodeposition; (c) and (d) metal deposit surface after mask removal, (c) deposit thickness is smaller than the spherical particle radius and (d) deposit thickness is equal to the spherical particle radius

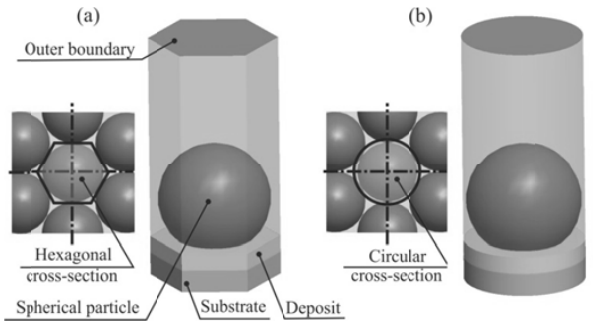

Fig. 2. (a) Arrangement of spherical particles in the colloidal crystal mask and unit cell with a regular hexagonal cross-section, (b) axisymmetric approximation of unit cell

In the dimensionless variables, the mathematical model of the process can be written as follows:

$$\frac{\partial^2\Phi}{\partial X^2}+\frac{\partial^2\Phi}{\partial Y^2}+\frac{\partial^2\Phi}{\partial Z^2}=0 \quad (5)$$

$$\frac{\partial Z_c}{\partial\tau}=\frac{\partial\Phi}{\partial N}\sqrt{1+\left(\frac{\partial Z_c}{\partial X}\right)^2+\left(\frac{\partial Z_c}{\partial Y}\right)^2} \quad (6)$$

The following equations are used as the boundary conditions:

$$\Phi\big|_C=0,\ \left.\frac{\partial\Phi}{\partial N}\right|_U=1,\ \left.\frac{\partial\Phi}{\partial N}\right|_I=0 \quad (7)$$

The initial conditions correspond to the initial plane surface of metal substrate:

$$Z_c(X,Y,0)=0. \quad (8)$$

The modeling is performed in the quasi-steady-state approximation: the distribution of potential is calculated ignoring the deposit surface motion due to the metal electrodeposition; the deposit surface evolution is calculated using the distribution of potential, which was obtained at the previous step. Thus, at each time step:

- the distribution of current density over a unit cell is calculated by solving the Laplace equation;
- new position of metal deposit surface is determined by solving equation (6).

3. Method of numerical modeling

The Laplace equations were solved numerically by the boundary element method. The advantage of the method is the simplicity of remeshing, when the geometry of computational region changes. In this case, the Laplace equation reduced to he boundary integral equation:

$$c\Phi(\mathbf{q})=-\int_\Gamma F(\mathbf{q},\mathbf{p})\Phi(\mathbf{p})d\Gamma+\int_\Gamma G(\mathbf{q},\mathbf{p})\frac{\partial\Phi}{\partial\mathbf{N}}d\Gamma \quad (9)$$

The numerical solution of equation (5) was performed by the convenient boundary element method (the computational volume varied from N^2 to N^3 depending on the method of solution of system of linear algebraic equations).

$$c\Phi_k=\sum_{m=1}^{N}F_{km}\Phi_m+\sum_{m=1}^{N}G_{km}\left(\frac{\partial\Phi}{\partial\mathbf{N}}\right)_m \quad (10)$$

where $F_{km}=-\int_{\Gamma_m}F(\mathbf{q}_k,\mathbf{p})d\Gamma,\quad G_{km}=\int_{\Gamma_m}G(\mathbf{q}_k,\mathbf{p})d\Gamma$.

The convenient boundary element method does not allow one to use sufficiently fine meshes, which provide sufficient accuracy of calculation of potential distribution. Therefore, a fast multipole boundary element method was used (the

computational volume varied from N to N^2 depending on the method of solution of system of linear algebraic equations) [20]. In the case of application of fast multipole boundary element method, the coefficients of the system of discrete equations were determined by the following equations:

$$G(\mathbf{q},\mathbf{p}) \approx \frac{1}{4\pi}\sum_{n=0}^{\infty}\sum_{m=-n}^{n}\overline{S}_{n,m}(\mathbf{q}-\mathbf{p}_c)R_{n,m}(\mathbf{p}-\mathbf{p}_c),$$
$$F(\mathbf{q},\mathbf{p}) \approx \frac{1}{4\pi}\sum_{n=0}^{\infty}\sum_{m=-n}^{n}\overline{S}_{n,m}(\mathbf{q}-\mathbf{p}_c)\frac{\partial R_{n,m}(\mathbf{p}-\mathbf{p}_c)}{\partial \mathbf{N}} \quad (11)$$

where $S_{n,m}(\mathbf{q}) = (n-m)!P_n^m(\cos\theta)e^{im\phi}r^n$, $R_{n,m}(\mathbf{q}) = \frac{1}{(n+m)!}P_n^m(\cos\theta)e^{im\phi}\frac{1}{r^{n+1}}$; $\mathbf{p}_c$ is the basic point of expansion; r,θ,ϕ are the coordinates of point $\mathbf{q}$ in the spherical system of coordinates; P_n^m is the associated Legendre function; $|\mathbf{p}-\mathbf{p}_c| < |\mathbf{q}-\mathbf{p}_c|$.

The equation of deposit surface evolution was solved numerically using the "Level Set" method [21]. The discrete form of equation (6) on the mesh of equilateral triangular elements can be written as follows:

$$Z_{c,k}^{n+1} = Z_{c,k}^{n} + \Delta\tau\left(\frac{\partial\Phi}{\partial N}\right)_k^n\sqrt{1+\left(\frac{\partial Z_c}{\partial X}\right)_{k,L}^2+\left(\frac{\partial Z_c}{\partial X}\right)_{k,R}^2+\left(\frac{\partial Z_c}{\partial Y}\right)_{k,L}^2+\left(\frac{\partial Z_c}{\partial Y}\right)_{k,R}^2} \quad (12)$$

The derivatives with respect to the spatial coordinates in equation (12) were calculated by the following equations:

$$\left(\frac{\partial Z_c}{\partial X}\right)_{k,L} = \max\left(\frac{Z_{c,k}^n - Z_{c,XL_k}^n}{X_k - X_{XL_k}},0\right)$$
$$\left(\frac{\partial Z_c}{\partial X}\right)_{k,R} = \min\left(\frac{Z_{c,XR_k}^n - Z_{c,k}^n}{X_{XR_k} - X_k},0\right) \quad (13)$$
$$\left(\frac{\partial Z_c}{\partial Y}\right)_{k,L} = \max\left(\frac{Z_{c,k}^n - 0.5\left(Z_{c,YLW_k}^n + Z_{c,YLO_k}^n\right)}{Y_k - 0.5\left(Y_{YLW_k} + Y_{YLO_k}\right)},0\right)$$
$$\left(\frac{\partial Z_c}{\partial Y}\right)_{k,R} = \min\left(\frac{0.5\left(Z_{c,YRW_k}^n + Z_{c,YRO_k}^n\right) - Z_{c,k}^n}{0.5\left(Y_{YRW_k} + Y_{YRO_k}\right) - Y_k},0\right)$$

Equations (13) are the generalization of the known equations of the "Level Set" method for the finite-difference mesh. As it is seen from Fig. 3, in the case of the mesh of equilateral triangular elements, the approximation of derivatives with respect to the X axis can be performed using directly the equations for the finite-difference mesh, whereas the approximation of derivatives with respect to the Y axis requires the use of a mean value for two neighboring nodes (YWR and YRO or YLW and YLO).

After each time step, the remeshing on the side surfaces of computational region was performed.

4. Results and discussion

The numerical solution of boundary value problem (5), (7) was performed by the boundary element method. The mesh parameters were chosen so that the calculated results were independent of the mesh step and the number of nodes. It was found that a mesh containing from 5000 to 20000 boundary elements should be used depending on a spherical particle packing (Fig. 4). On the surfaces corresponding to the metal deposit and outer boundary of computational region, the equilateral triangular boundary elements formed. On the side surfaces of computational region, the boundary elements in the shape of right angled triangles were used; in order to eliminate the effect of mesh on the distribution of potential, the element height was decreased as the deposit surface was approached.

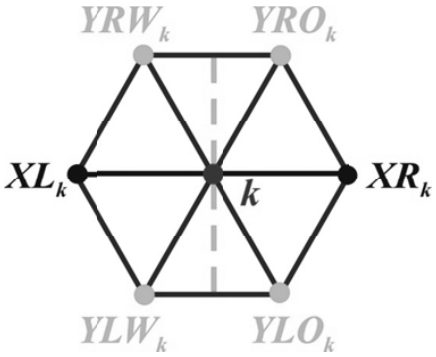

Fig. 3. Scheme of approximation of derivatives with respect to the spatial coordinated on the mesh of equilateral triangular elements by the "Level Set" method

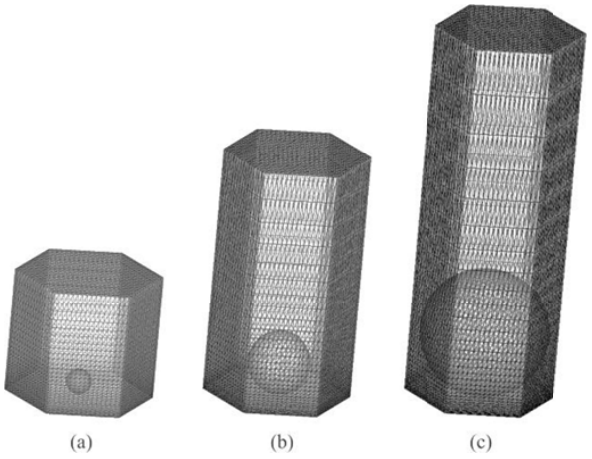

Fig. 4. Scheme of partitioning computational region into boundary elements: (а) R=0.1; (б) R=0.25; (в) R=0.5

At the second stage, the modeling of metal deposit growth was realized at various spherical particle packing densities (Fig. 5).

In the course of cathodic deposition, nearly axisymmetric nanoprojections form on the substrate surface. When the packing density of spherical particles decreases (R decreases), a deviation from the axis symmetry also decreases. The height of nanoprojections increases with the time.

The used explicit coordinate presentation of deposit surface allows us to simulate the electrodeposition only at

the deposit thickness not exceeding R. If it is necessary to consider a larger thickness of metal deposit layer, the following equation can be used as the initial condition instead of equation (8):

$$Z_c(X,Y,0) = R. \quad (14)$$

As a result of modeling, the rate of deposit growth in the pores between the spherical particles of MCC mask and the time dependence of metal deposit shape were determined. In addition, the potential difference between the growing metal deposit layer and the outer (upper) boundary of computational region was calculated. The results of modeling also enabled us to determine the time taken to obtain the deposit of the prescribed thickness. In the course of electrodeposition, the active surface area varies leading to the variation of the rate of metal layer deposition. At the deposit thickness smaller than R, the rate of deposition increases with the time. At the deposit thickness larger than R, the deposition rate decreases with the time. The proposed scheme of modeling enables one to determine quantitatively the time dependence of deposition rate, which can be used to choose the conditions of metal electrodeposition.

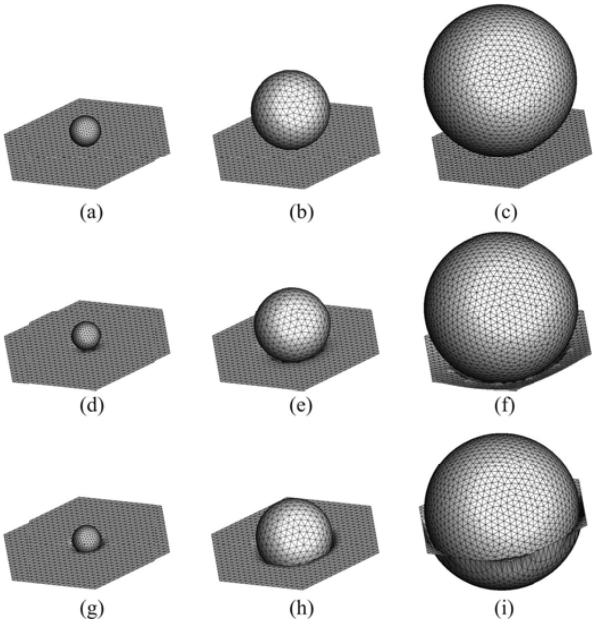

Fig. 5. Results of modeling of metal electrodeposition through MCC mask at various radii of spherical particles: (a, d, g) R=0.1; (b, e, h) R=0.25; (c, f, i) R=0.5; (a, b, c) before electrodeposition; (d, e, f) at the thickness of deposit equal 0.4R; (g, h, i) at the thickness of deposit equal 0.8R

In view of the fact that the deposit surface in a unit cell is nearly axisymmetric, the computational experiments were performed within the axisymmetric approximation. This allowed us to reduce significantly the volume of computation. Fig. 6 gives the results of modeling for several radii of spherical particles. The arrow in Fig. 6 shows the curves, which correspond to various instants of time with a step $\Delta\tau$=0.01. If necessary, the dimensional time can be determined by equation (4).

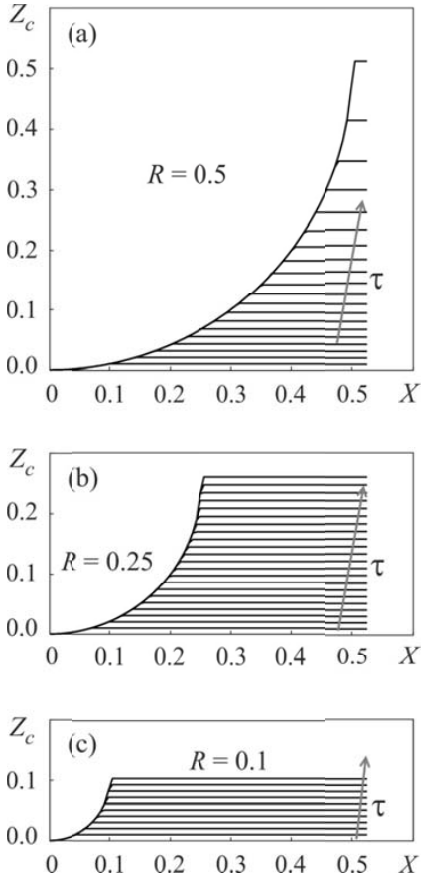

Fig. 6. Results of modeling within the axisymmetric approximation of metal electrodeposition through MCC mask at various radii of spherical particles: (a) R=0.5; (b) R=0.25; (c) R=0.1

In the case of dense packing of spherical particles (R=0.5), the metal deposition rate increases most steeply (Fig. 6a), whereas in the case of low-density packing (R=0.1), the rate of metal deposition insignificantly increases with increasing deposit thickness (Fig. 6c).

The simulated dependences of the potential on the deposit thickness agree with the experimental data: the potential increases with decreasing electroactive surface area.

Conclusions

The proposed mathematical model of transport processes in the metal electrodeposition through colloidal crystal mask is based on the quasi-steady-state approximation. The dependences of an average current density (deposit growth rate) on the thickness of deposited metal layer (time) were obtained. In particular, the model enables us to obtain the quantitative dependences between the thickness of deposited metal layer, the operating conditions, and the current density.

It is found that the surface of growing deposit is nearly axisymmetric; therefore, the axisymmetric approximation

may be used. The proposed scheme of modeling can be used to organize and optimize the processes of electrodeposition through the MCC mask.

Acknowledgements

This work was supported by the Russian Foundation for Basic Research, project no. 13-03-00537 and the Ministry of Education and Science of the Russian Federation, project no. 1096 of the Basic Part of the State Program.

References

[1] Bruzzone AAG, Costa HL, Lonardo PM, Lucca DA. Advances in engineered surfaces for functional performance. CIRP Ann-Manuf Techn 2008;57(2):750-769.
[2] De Chiffre L, Kunzmann H, Peggs GN, Lucca DA. Surfaces in precision engineering, microengineering and nanotechnology. CIRP Ann-Manuf Techn 2003;52(2):561-577.
[3] Malshe A, Rajurkar K, Samant A, Hansen HN, Bapat S, Jiang W. Bio-inspired functional surfaces for advanced applications. CIRP Ann-Manuf Techn 2013;62(2):607-628.
[4] Huczko A. Template-based synthesis of nanomaterials. Appl Phys A-Mater 2000;70(4):365-376.
[5] Xia Y, Yang P, Sun Y, Wu Y, Mayers B, Gates B, Yin Y, Kim F, Yan H. One-Dimensional Nanostructures: Synthesis, Characterization, and Applications. Adv Mater 2003;15(5):353–389.
[6] Liu R, Duay J, Lee SB. Heterogeneous nanostructured electrode materials for electrochemical energy storage. Chem Commun 2011;47:1384–1404.
[7] Wade TL, Wegrowe J-E. Template synthesis of nanomaterials. Eur Phys J-Appl Phys 2005;29(1):3-22.
[8] Proenca MP, Sousa CT, Ventura J, Vazquez M, Araujo JP. Ni growth inside ordered arrays of alumina nanopores: Enhancing the deposition rate. Electrochim. Acta 2012;72:215-221.
[9] Leprince-Wang Y, Bouchaib S, Brouri T, Capo-Chichi M, Laurent K, Leopoldes J, Chen Y. Fabrication of ZnO micro- and nano-structures by electrodeposition using nanoporous and lithography defined templates. Mat Sci Eng B-Solid 2010;170(1-3):107-112.
[10]. Lahav M, Weiss E, Xu Q, Whitesides GM. Core-Shell and Segmented Polymer-Metal Composite Nanostructures. Nano Lett 2006;6:2166–2171.
[11] Velev OD, Lenhoff AM. Colloidal crystals as templates for porous materials. Curr Opin Colloid In 2000;5:56-63.
[12] Stein A. Sphere templating methods for periodic porous solids. Micropor Mesopor Mat 2001;44-45:227-239.
[13] Zhang J, Li Y, Zhang X, Yang B. Colloidal Self-Assembly Meets Nanofabrication: From Two-Dimensional Colloidal Crystals to Nanostructure Arrays. Adv Mater 2010;22(38):4249-4269.
[14] Ye X, Qi L. Two-dimensionally patterned nanostructures based on monolayer colloidal crystals: controllable fabrication, assembly, and applications. Nano Today 2011;6(6):608-631.
[15] Jiang P. Large-scale fabrication of periodic nanostructured materials by using hexagonal non-close-packed colloidal crystals as templates. Langmuir 2006;22(9):3955-3958.
[16] Bartlett PN, Baumberg JJ, Birkin PR, Ghanem MA, Netti MC. Highly ordered macroporous gold and platinum films formed by electrochemical deposition through templates assembled from submicron diameter monodisperse polystyrene spheres. Chem Mater 2002;14:2199-2008.
[17] Spada ER, Da Rocha AS, Jasinski EF, Pereira GMC, Chavero LN, Oliveira AB, Azevedo A, Santorelli ML. Homogeneous growth of antidot structures electrodeposited on Si by nanosphere lithography. J Appl Phys 2008;103:114306.
[18] Newton MR, Morey KA, Zhang Y, Snow RJ, Diwekar M, Shi J, White HS. Anisotropic Diffusion in Face-Centered Cubic Opals. Nano Lett 2004;4:875-880.
[19] Volgin VM, Davydov AD, Kabanova TB. Calculation of effective diffusion coefficient in a colloidal crystal by the finite element method. Russ J Electrochem 2012;48:817-834.
[20] Liu Y. Fast multipole boundary element method: theory and applications in engineering. Cambridge University Press; 2009.
[21] Osher S, Sethian JA. Fronts propagating with curvature-dependent speed: algorithms based on Hamilton-Jacobi formulations. J Comput Phys 1988;79(1):12-49.